Journal of Natural Gas Science and Engineering 35 (2016) 614–623

Contents lists available at ScienceDirect

Journal of Natural Gas Science and Engineering

journal homepage: www.elsevier.com/locate/jngse

# CDEM-based analysis of the 3D initiation and propagation of hydrofracturing cracks in heterogeneous glutenites

Yang Ju [a, b, *], Peng Liu [c], Jialiang Chen [c], Yongming Yang [c], Pathegama G. Ranjith [d]

[a] State Key Laboratory for Geomechanics & Deep Underground Engineering, China University of Mining & Technology, No. 1 University Avenue, Xuzhou 221116, China
[b] State Key Laboratory of Coal Resources & Safe Mining, China University of Mining & Technology at Beijing, D11 Xueyuan Road, Beijing 100083, China
[c] School of Mechanics and Civil Engineering, China University of Mining & Technology at Beijing, D11 Xueyuan Road, Beijing 100083, China
[d] Department of Civil Engineering, Monash University, Clayton, Melbourne, Victoria 3800, Australia

ARTICLE INFO

*Article history:*
Received 12 June 2016
Received in revised form
1 September 2016
Accepted 5 September 2016
Available online 8 September 2016

*Keywords:*
Hydrofracturing
Numerical simulation
Heterogeneity
CDEM
Crack initiation
Crack propagation process

ABSTRACT

Unconventional natural gas reservoirs usually have composite or heterogeneous microstructures, and heterogeneity has significant influence on the initiation and propagation of hydrofracturing cracks. Numerical simulation has advantages over in situ or experimental studies in the examination of the integrate hydrofracturing process. Many numerical modelling studies have been conducted to investigate the patterns of underground hydraulic fracturing. Unfortunately, few models have adequately simulated the 3D dynamic hydraulic fracturing process while maintaining accurate heterogeneous structures. This study adopted numerical simulation to investigate the processes of the initiation and the propagation of cracks in a heterogeneous material based on the CDEM algorithm, which couples finite and discrete element methods. A numerical model was used to represent the actual heterogeneous structure of a physical specimen. The initiation position and process of propagation of cracks influenced by geostress differences and heterogeneity are discussed. The efficiency of the simulation work was verified by the 3D reconstruction models in terms of the experimental results. The results indicated that material heterogeneity has considerable effect on crack initiation, but that crack propagation is controlled primarily by the geostress ratio.



## 1. Introduction

Hydrofracturing is one of the primary techniques adopted for the stimulation of unconventional natural gas reservoirs. Such reservoirs usually have composite or heterogeneous microstructures that can be seen with the naked eye or observed by detection methods (Fouche et al., 2004; He et al., 2015). Glutenite is a representative heterogeneous rock medium that is widely found in tight gas reservoirs (Liu et al., 2010; Zhang et al., 2014). It is evidenced that the initiation and growth behaviors of hydrofracturing cracks are strongly influenced by the heterogeneity of rock or rocklike materials (Renard et al., 2009; Sarmadivaleh and Rasouli, 2015). Consequently, fracture patterns obtained in the field or by experiment usually deviate from theoretical predictions, which might assume homogenous rock material around the wellbore or in one pay zone. Understanding the mechanisms of the initiation and growth of hydrofracturing cracks associated with the heterogeneity of rock material is pivotal in enhancing hydraulic fracturing stimulation.

In situ monitoring and laboratory tests have been conducted to identify the morphologies of hydrofracturing cracks in rock materials. Many of these studies have observed and recorded crack morphologies after the completion of hydraulic fracturing tests using microseism technology or nondestructive testing (Adriaensens et al., 2000; Bunger et al., 2015; Chen et al., 2015; Cipolla et al., 2012; Gomaa et al., 2014; Guo et al., 2015; Gutierrez et al., 2010; Hampton et al., 2014; Ju et al., 2016; Zou et al., 2016). However, the fracture initiation and growth processes are usually indistinct in such studies. In fact, complex hydrofracturing crack geometry reflects the development of material dilatancy and brittle failure with reference to crack nucleation, propagation, and coalescence.

Because of the difficulty in obtaining a complete analysis

* Corresponding author. State Key Laboratory of Coal Resources & Safe Mining, China University of Mining & Technology, D11 Xueyuan Road, Beijing 100083, China.
*E-mail address:* juy@cumtb.edu.cn (Y. Ju).

http://dx.doi.org/10.1016/j.jngse.2016.09.011
1875-5100/

solution for hydrofracturing problems, numerical methods are widely adopted. The rapid development of 2D and 3D numerical models has advanced the simulation of the initiation and propagation of complex hydrofracturing cracks (Dong and De Pater, 2001; Hiyama et al., 2013; Nassir et al., 2010; Zhang et al., 2007). However, in most cases, to simplify the numerical computation, the heterogeneity of the rock formation has been ignored. This has been proven to cause deviations between the simulated and actual crack morphology. Hydraulic fracturing behavior reflects the influence of both the geostress field and the heterogeneity of the rock media, and different techniques have been used to incorporate heterogeneity into numerical models. Heterogeneity adopting some kind of distribution has been implemented in some homogeneous models. This procedure assigns different properties to the elements within the model. For example, the FSD model considers the sample as a single uniform material and it uses the Weibull statistical model to introduce rock heterogeneity (Li et al., 2013; Tang et al., 2002; Wong et al., 2006; Yang et al., 2004). Alternatively, accurate material heterogeneity is introduced into some models by means of digital image processing. For example, classified mineral maps have been used to construct finite element meshes (Liu et al., 2004; Wang, 2013; Yue et al., 2003). Furthermore, the discrete element method (DEM) can directly represent the grain-scale microstructural features of granular materials by considering each grain as a DEM particle (Cundall and Strack, 1979; Potyondy and Cundall, 2004). Therefore, particles can be assigned different mechanical parameters to generate model heterogeneity (Al-Busaidi et al., 2005; Fatahi et al., 2016; Shimizu et al., 2011, 2014). All these methods have contributed to the characterization of the heterogeneity of rock material and to the realization of fracturing patterns in heterogeneous media. However, approaches that consider rock heterogeneity follows some statistical laws cannot reflect the actual distribution of mineral components distribution nor take into account the effects of interfaces between inclusions and matrices (Li et al., 2015). Some traditional numerical models, such as those that adopt the finite element method (FEM), have some major limitation; their meshes cannot be changed easily after creation and they require further assumptions and simplifications. DEM model is a tool that does not require meshing because it consists of discretized particles free to move with respect to each other. However, it is a challenge to implement actual components distributions in DEM models. Moreover, to the best of our knowledge, few works have reported robust numerical evidence of a relationship between crack patterns and the heterogeneity of rock materials.

The purpose of this study was to investigate the coupling effect of heterogeneity and geostress contrast on the initiation and propagation behaviors of hydrofracturing cracks. This was achieved using a continuum-based discrete element method (CDEM) model that couples the FEM and DEM and has advantages in simulating 3D discontinuous deformation problems. The models were constructed with accurate inner structures of the rock material based on computed tomography image processing methods. The effects of material heterogeneity and in situ geostress difference on hydraulic fracturing behavior were investigated through a series of boundary conditions. The initiation positions and propagation processes of the cracks influenced by geostress differences and heterogeneous gravels were analyzed by applying appropriate loading steps. The final crack morphology was verified by experimental results.

The remainder of this paper is organized as follows. In Section 2, the numerical simulation conditions, including the CDEM algorithm boundary conditions and calculation steps are introduced in detail. Section 3 outlines the numerical results and the analysis of the 3D crack growth and distribution in heterogeneous rock media. In Section 4, the experimental results are employed to verify the final crack morphologies. Concluding remarks are summarized in Section 5.

## 2. Numerical simulation for hydrofracturing crack propagation

### 2.1. CDEM algorithms

The CDEM algorithm couples the FEM and the DEM (Li et al., 2004; Wang et al., 2005). A microstructural model of rock material comprises two elements: block elements and jointed elements. The model is configured such that the FEM is used inside the block, while the DEM is adopted for the interface. Moreover, the strength of each element is relevant to its deformation modulus, and the deformation of each block element is obtained according to the state of stress and constitutive relation of the materials. Various elements are available in a CDEM model, e.g., tetrahedral, hexahedral, or even complex polyhedral elements. This method has considerable advantage in simulating dynamic fracture processes, and it has a variety of applications related to problems associated with continuous or discontinuous deformation under dynamic or static loads.

The governing equation for the moving of the movement of elements is the motion equation that takes the deformation of elements into account. For every block within the model, the following governing equations must be satisfied.

Equilibrium equation:

$$\sigma_{ij,j} + f_i - \rho \ddot{u}_i - \alpha \ddot{u}_i = 0 \tag{1}$$

where $\sigma_{ij,j}$ represents the first-order partial derivative of the stress tensor with respect to the coordinate; $f_i$ stands for the body force; $\rho$ is density; $\alpha$ is the damping ratio; and $\ddot{u}_i$ and $\dot{u}_i$ denote acceleration and velocity respectively.

Using the variation formulation, the equilibrium equation can be transformed into the following matrix form in an element:

$$M\ddot{u}(t) + C\dot{u}(t) + Ku(t) = Q(t) \tag{2}$$

where $M$, $C$, and $K$ are the mass, damping and stiffness matrices, respectively, $\ddot{u}(t)$, $\dot{u}(t)$, and $u(t)$ denote vectors containing the nodal accelerations, displacements, and velocities at time point t, respectively; and $Q(t)$ is the loading vector. To use the dynamic relaxation method to solve the equation, CDEM employs an explicit iteration in the calculation.

Strain-displacement relationship:

$$\varepsilon_{ij} = \frac{1}{2}\left(u_{i,j} + u_{j,i}\right) \tag{3}$$

Constitutive law:

$$\sigma_{ij} = D_{ijkl}\varepsilon_{kl} \tag{4}$$

Boundary conditions:

$$u_i = \overline{u}_i, \quad \sigma_{ij}n_j = \overline{t}_i \tag{5}$$

Initial conditions:

$$u_i(x,y,z,0) = u_i^0(x,y,z), \quad u_{i,t}(x,y,z,0) = u_{i,t}^0(x,y,z) \tag{6}$$

In Eqs. (3)–(6), $u_{i,j}$, and $u_{j,i}$ are both the first-order partial derivatives of displacement with respect to the coordinate; $\varepsilon_{ij}$ and $\varepsilon_{kl}$ are strains; $\sigma_{ij}$ is stress; and $D_{ijkl}$ is the stress—strain tensor.

The failure, slipping, and fracture of the solid occur in the interface between elements. Two criteria are used to judge the failure of the elements:

(1) Maximum Tensile-Stress Criterion:

$$\sigma_T \geq \overline{\sigma}_T \tag{7}$$

(2) Mohr-Coulomb Strength Theory:

$$\tau \geq \sigma_n \tan\varphi + C \tag{8}$$

where $\overline{\sigma}_T$ is the tensile strength, $C$ is cohesion, and $\varphi$ is the internal friction angle.

Fig. 1 shows a diagram of the fracture process in the CDEM algorithm. The solid is meshed by tetrahedral elements. If either of the above criteria were satisfied, the solid would rupture by separating at the mass point. This means that cracks cannot get access into the elements.

External loads are treated using the stiffness matrix method as follows:

$$\{F\}_i^e = [K]_i^e \cdot \{u\}_i^e \tag{9}$$

where $\{F\}_i^e$ is the node forces vector of element $i$, while $\{u\}_i^e$ denotes the node displacement vector, and $[K]_i^e$ refers to the stiffness matrix. $\{F\}_i^e$ can be obtained by

$$\begin{cases} F_n^j = -K_n^j \times \Delta d_n^j \\ F_s^j = -K_s^j \times \Delta d_s^j \end{cases} \tag{10}$$

where $F_n^j$ and $F_s^j$ are the normal or tangential node force vectors of element $j$, $K_n^j$ and $K_s^j$ are the normal or tangential stiffness matrices of element $j$, and $\Delta d_n^j$ and $\Delta d_s^j$ are the normal or tangential displacement vectors of element $j$.

To make the calculation more efficient when the number of elements is a large, parallel computing is employed in the CDEM algorithm. The CPU (Central Processing Unit) in the CDEM solver was substituted by the GPU (Graphics Processing Unit). The GPU that has specialized electronic circuitry designed to rapidly manipulate and alter memory is used to accelerate the creation of images in a frame buffer intended for output to display (Wang et al., 2013). The CDEM algorithm is suitable for application with a GPU because the calculations involved are all preformed independently for each of the elements and nodes. In this case, the CDEM is denoted as GDEM. In GPU parallelization, heterogeneous computing methodology is usually used. This means that the serial part of the code executes in a host (CPU) thread, while the parallel part executes in a large number of device (GPU) threads. In our work, the GDEM solver was adopted for the models comprising millions of elements which might require one week to complete the computation using traditional CPU algorithms, and as a result, the computation time was shortened to half an hour.

### 2.2. Numerical model

In order to identify the effect of heterogeneity on hydrofracturing behavior, our previous work constructed a series of experimental models in terms of the characterizations of gravels in natural heterogeneous glutenite (Ju et al., 2016). According to the experimental settings and conditions, the same geometry and components settings were employed in the numerical model based on the assumption the heterogeneous model comprised an isotropic matrix and randomly distributed irregular gravels. A numerical model had side lengths of 100 mm. A 10-mm-diameter vertical hole with a length of 27 mm was drilled in the center of a cubic specimen, and an impermeable steel packer with a depth of 25 mm was set on the top of the open hole to seal fluid in the hole. Fig. 2 diagrams the geometry and setup of the model.

The numerical models were constructed in accord with the geometry and mechanical properties of the natural glutenite specimens with an identical gravel fraction of 28.5%. The geometrical characterizations as well as the mechanical properties of the natural glutenite specimens were first acquired using X-ray CT and mechanical tests and then used to reconstruct numerical models through MIMICS© and CDEM codes. In this study, the degree of material heterogeneity is defined by the proportion of the volume

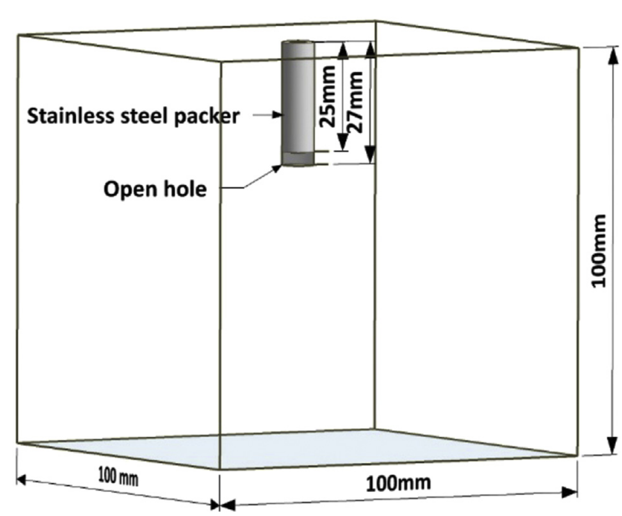


**Fig. 2.** Schematic of the numerical model for triaxial hydrofracturing.

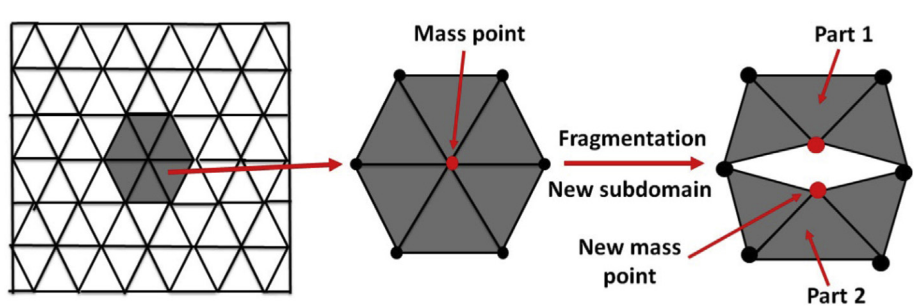


**Fig. 1.** Schematic of element separation.

of gravels to the volume of an entire heterogeneous specimen. It means that the distribution characterizations of gravel size and spatial location as well as gravel compositions are identical between each model, except the characterization of gravel quantity. A few factors cause us to take different initial distribution of heterogeneity. First, this measure facilitates validation of the CDEM simulation results using experimental data. The different distribution of heterogeneity results from the distinct gravel distribution of real glutenite samples. Second, we mainly focused on the effect of various gravel fractions on the hydrofracturing crack initiation and propagation behavior of a heterogeneous model subject to a constant geostress difference. Previous studies indicate that different spatial locations of gravels that are characterized by identical distribution functions of size, quantity and location have very little influence on the mechanical properties of the material (Liu et al., 2004; Yin et al., 2016). The experimental results of the natural rock cores that were drilled from the same reservoir but different spots indicated the rock samples had very close mechanical properties even though their graveled structures appeared different.

The computational model was constructed as follows. First, we detected the inner structure of the experimental specimens by means of X-ray CT. Furthermore, taking the assumption mentioned above into account, the original CT images were digitalized into images that comprised only the pixels of the matrix and the gravels using multi-thresholding segmentation method (Kaestner et al., 2008) and our own self-developed computer program (Ju et al., 2013, 2014). Thus, a 3D numerical model was constructed using MIMICS© software (http://biomedical.materialise.com/mimics) based on a set of processed 2D images, in which the pixel size was 0.144 mm and the interval between the slices was also 0.144 mm. After being reconstructed, the three-dimensional geometrical model was meshed using the mesh generation function of MIMICS©. Most numerical studies pointed out that mesh size affected simulation accuracy and efficiency (Bouchard et al., 2000; Moës et al., 1999; Rashid, 1998). In this study, to achieve a high computing accuracy and efficiency simultaneously, the element meshes in the vicinity of the wellbore were refined using MIMICS© according to actual sizes of gravels. The maximum side length of elements actually varies in the areas between the vicinity of the wellbore and the border of the model. Fig. 3 shows the different maximum side lengths of elements ranging between 0.5 mm and 2 mm. As a result, we obtained a meshed model composite of more than 800,000 elements that were divided into two groups: the matrix and the gravels. The meshed three-dimensional model was exported as a CDB file, compatible for mesh refinement and optimization using ANSYS© software. The meshed model was refined using the ANSYS software by employing self-developed code before being input into the GDEM solver, because errors would occur if the CDB file were used directly in the GDEM solver. Fig. 4 demonstrates this procedure.

In the calculation model, different mechanical parameters were assigned to the elements according to their association as matrix or gravels. All gravels were assigned the same mechanical parameters. It should be noted that the purpose of this study is to numerically analyze the effect of heterogeneity, which is weighed by gravel volumetric fraction, on hydrofracturing behavior of a heterogeneous rock. Therefore, the mechanical properties of gravels were set to be identical in our numerical simulation. In addition, as aforementioned, for the purpose of comparison, the CDEM models were actually constructed in accord with the geometry and mechanical properties of the natural glutenite specimens that were used in hydrofracturing experiments. Our preliminary experiments of the mineral compositions of gravels in the natural glutenite samples show that dolomite is predominant mineral composition of gravels (Liu et al., 2016; Ju et al., 2016). Therefore, to address the effect of gravel existence instead of gravel mineral composition on the hydrofracturing behavior of heterogeneous models, we assigned the mechanical properties of dolomite to all gravel elements in our model. Table 1 lists all the parameters used in simulation.

### 2.3. General procedure

To probe the effects of geostress difference in various directions on hydraulic fracturing, the boundaries of the elements were set as pressure conditions. The various stresses were applied to the model along the principal stress directions. In this study, we adopted the same setting of geostress conditions as in our previous works. Five groups of horizontal geostress ratios were employed within the range from 1:1.0 to 1:1.9. Table 2 displays the parameters of the stresses used in the simulation.

The general procedure of the numerical simulation performed using the GDEM solver was as follows. The boundary stresses were applied to achieve an initial stress balance. Furthermore, in order to simulate the actual process of increasing water pressure in the wellbore, the pressure continuously increased step by step with an interval of 5 MPa until the specimen was split out. As a result, the pressure on the crack surface increased steadily. Water injection was not considered as a time-dependent process (Almi et al., 2014). This was designed to be in line with the water injection process that was adopted in our previous experiments for comparison purposes (Liu et al., 2016; Ju et al., 2016). The purpose of adopting stepwise loading methods in simulation is to reveal how fractures initiate and propagate step by step within a rock specimen which is difficult to be observed in hydraulic fracturing tests. A proper water pressure gradient not only helps achieve this goal but also facilitates

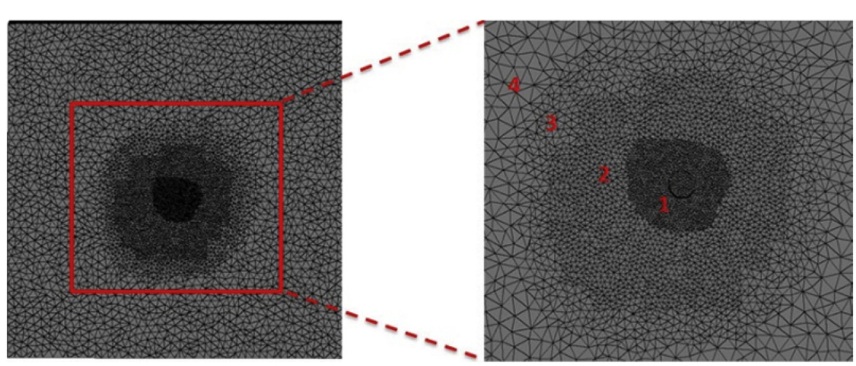


**Fig. 3.** Illustration of the refined meshes in the specific areas that are labeled by red number 1, 2, 3 and 4, of which the maximum side length is 0.5 mm, 1 mm, 1.5 mm, and 2 mm, respectively. (For interpretation of the references to colour in this figure legend, the reader is referred to the web version of this article.)

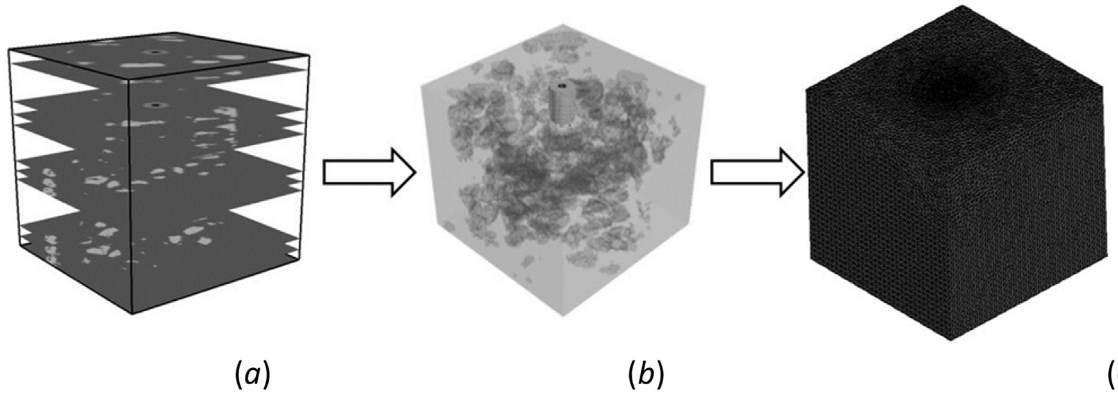


**Fig. 4.** Procedure of obtaining the meshed three-dimensional heterogeneous model based on the MIMICS and ANSYS codes, (***a***) stacking of 2D binarized CT images, (***b***) reconstructed model, and (***c***) meshed model.

**Table 1**
Mechanical parameters for the model.

| Components | Young's modulus E (GPa) | Poisson's ratio $\upsilon$ | Tensile strength $\sigma_t$ (MPa) | Cohesion C (MPa) | Frictional angle $\varphi$ (°) |
|---|---|---|---|---|---|
| Matrix | 22.29 | 0.14 | 15 | 52.44 | 26.13 |
| Gravel | 43.80 | 0.11 | 25 | 100 | 50 |

**Table 2**
Stress conditions set on the boundaries of the model elements.

| Model | $\sigma_H/\sigma_h$ | $\sigma_H$(MPa) | $\sigma_h$(MPa) | $\sigma_z$(MPa) |
|---|---|---|---|---|
| 1 | 1.0 | 10 | 10 | 20 |
| 2 | 1.3 | 13 | 10 | 20 |
| 3 | 1.5 | 15 | 10 | 20 |
| 4 | 1.7 | 17 | 10 | 20 |
| 5 | 1.9 | 19 | 10 | 20 |

numerical computation efficiency. In order to make the simulation of hydrofracturing easy to implement, as a preliminary attempt, we did not take account of the coupled effect of fluid flow and crack propagation in the simulation. We assumed that the water pressure along crack surfaces was uniform, i.e. no pressure gradient varying with crack propagation and water transport was counted. When either the maximum tensile stress criterion or the Mohr—Coulomb strength criterion was satisfied, a crack was initiated. The failure of joint elements at the initial crack tip was also decided by the maximum tensile stress criterion and the Mohr—Coulomb strength criterion, which forced the crack to propagate. In this study, the water pressure was applied in nine steps for all the models.

## 3. Results and discussion

To probe the coupling effects of heterogeneity and geostress difference on crack initiation and propagation processes, Fig. 5 illustrates (from left to right) the intact heterogeneous model, and crack morphologies in the initiation and propagation stages. It can be seen that the cracks did not emerge along the direction of maximum horizontal stress, as considered in conventional theory (Zhou et al., 2016) when the geostress ratio is < 1.7; instead, the cracks emerged at various azimuths around the vertical wellbore. This means that heterogeneous rock media provide additional possible weak positions for crack initiation and that the geostress ratio dominates crack propagation. Once the geostress ratio is > 1.7, the crack tended to initiate in the direction along the line of maximum horizontal geostress ratio. This scenario has been observed and discussed in our previous study (Liu et al., 2016). As pointed out, the crack initiation and propagation behavior is governed by the stress state of rock in the neighborhood of the borehole. The maximum circumferential stress theory assumes that crack initiates at the point where the circumferential stress reaches its maximum value, i.e. the equation $(\sigma_H - \sigma_h)sin2\beta = 0$ should be satisfied, where β is the fracture initiation angle. If there is no difference between the horizontal principal stresses, the fracture initiation angle can be an arbitrary value to satisfy the equation. Considering the actual strength difference of the glutenite at various locations, it is straightforward to understand that multiple cracks could emerge at different positions near the wellbore once the maximum circumferential stresses exceed the ultimate tensile strengths of the points of interest. In contrast, if $\sigma_H \neq \sigma_h$, the initiation fracture angle complies $sin2\beta = 0$, i.e. $\beta = 0^{\circ}$ or $\beta = 180^{\circ}$, which implies that the double-wing crack emerges along the maximum horizontal stress direction. This is in line with the observed facture pattern that a double-wing crack predominately emerges along the maximum horizontal stress direction as the geostress ratio is greater than 1:1.7. In fact, due to existence of heterogeneity of glutenite, the fracture initiation azimuth not only depends on stress difference but also depends on material heterogeneity. The heterogeneity leads to the non-uniform distribution of the material strengths, and accordingly affects the fracture initiation position and azimuth. The fracture initiation angle β falls within the range between 0° and 180°. This has been verified by the measured fracture patterns of the glutenite under the horizontal geostress ratio lower than 1:1.7. The ratio 1:1.7 appears to be the threshold stress ratio below which material heterogeneity rather than geostress difference plays the dominant role in governing initial crack propagation.

It is noteworthy that the magnitude of confining pressure apparently affects the mechanical parameters, such as compressive and tensile strengths, Young's modulus, and fracture toughness, of reservoir rocks (Hu et al., 2015; Morita et al., 1992), and therefore could impact their fracturing behavior. The obtained threshold stress ratio based on the current confining stress conditions could vary if the magnitude of the minimum stress changes. However, this study focuses on the effects of heterogeneity and confining stress difference on hydraulic fracturing behavior of reservoir rocks

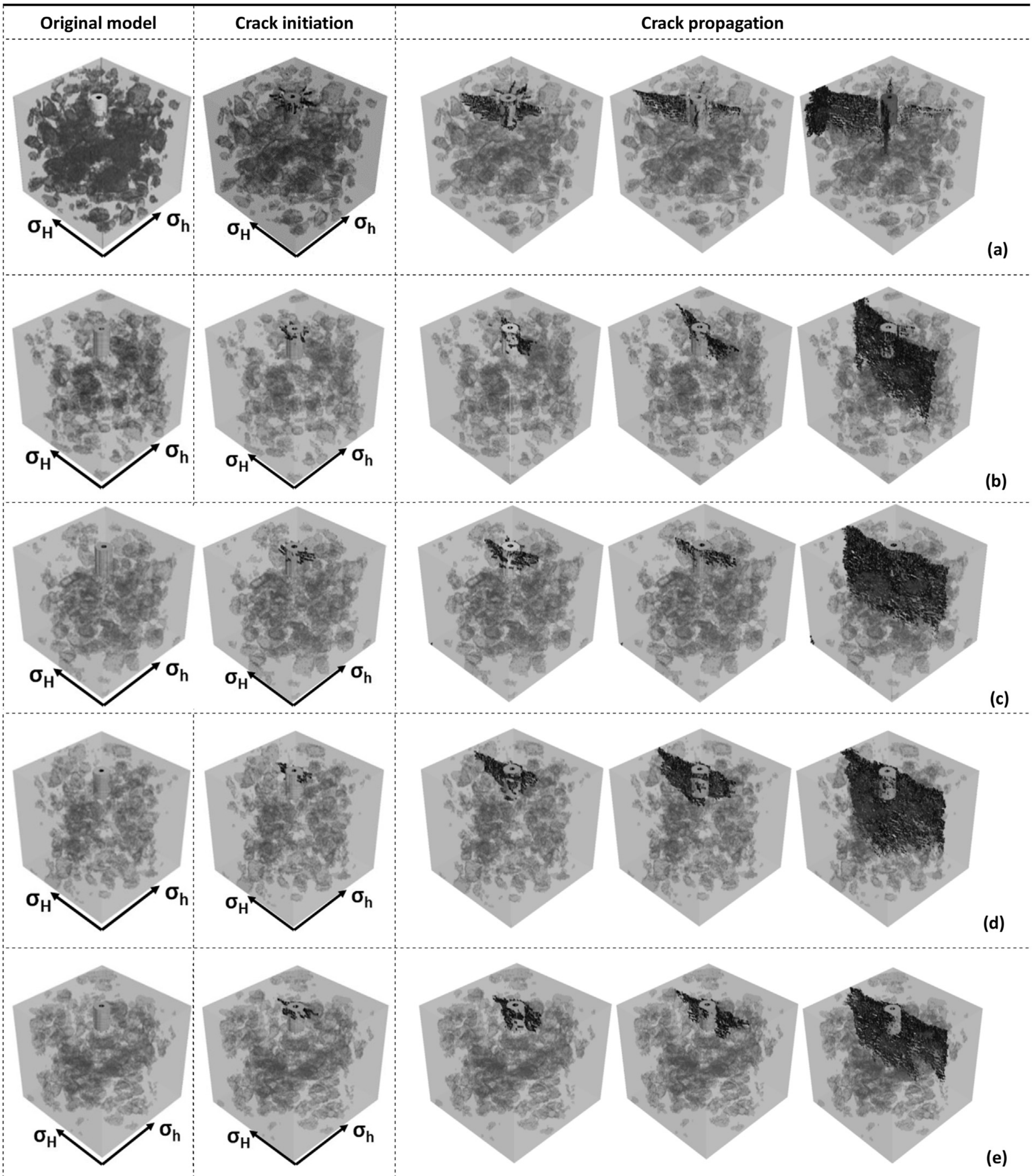


**Fig. 5.** 3D morphologies of hydrofracturing cracks in heterogeneous models under different loading steps. Rows (***a***) to (***e***) show the results for geostress ratios ranging from 1:1.0 to 1:1.9.

in accordance with the actual geostress range (Ju et al., 2016; Liu et al., 2016). The effect of the minimum stress on hydrofracturing behavior of rock can be further justified through laboratory tests.

It is shown that hydrofracturing cracks initiated from the upper part of the wellbore. To our knowledge, crack initiation highly depends on the stress state and equivalent strength of the rock element of interest. In our numerical models, the crack initiation in the vicinity of the wellbore is determined by the maximum circumferential tensile stress or the maximum shear stress, depending on whichever is achieved first, where the maximum circumferential tensile stress and Mohr-Coulomb strength criteria are applied. Fig. 6 illustrates the results of the X-direction and Y-direction components of the maximum circumferential tensile stress around the borehole. It is evident that the maximum circumferential tensile stresses of the rock elements around the upper part of the wellbore are higher than those of other regions. This explains the causes for crack initiation surrounding upper part of the wellbore.

In the crack propagation process, cracks in the upper of the wellbore were always ahead of those at the bottom. This implies

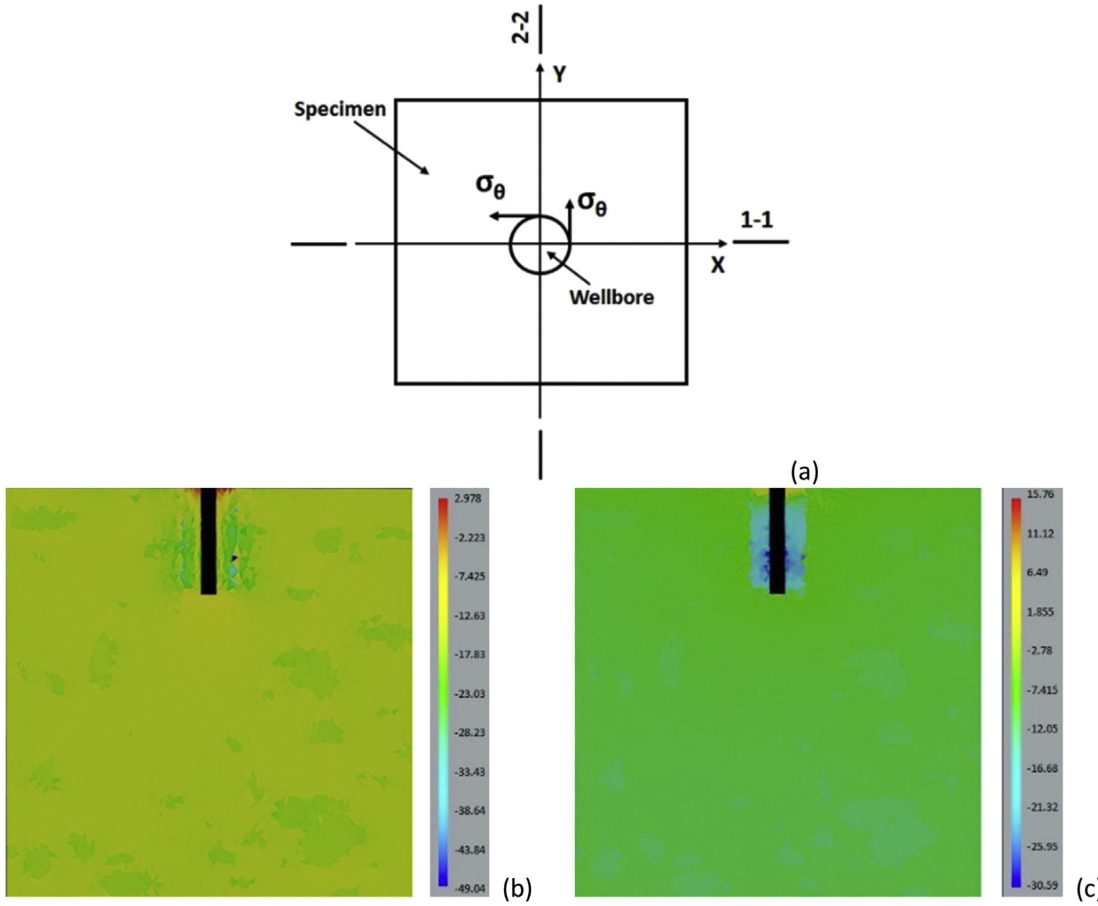


**Fig. 6.** Illustration of the maximum circumferential tensile stress around the wellbore (***a***), y-direction component along profile 1-1, (***b***), and x-direction components along the profile 2-2 (c).

that cracks generally initiate from the upper part of the wellbore surface and propagate vertically downward. It is evidenced that multiple, twisted cracks appeared when the horizontal geostress ratio was 1:1. In such circumstances, hydrofracturing cracks would propagate along the direction of initiation and form at least four branches. Nevertheless, it should be noted that once the geostress difference was no longer equivalent, the cracks preferred to propagate along the direction of maximum horizontal stress. When the geostress difference reached 1:1.7, the initial cracks coalesced to form a double-wing crack along the direction of maximum horizontal geostress, even though the cracks initiated in multiple directions around the wellbore.

To elucidate the effect of material heterogeneity on hydrofracturing behavior, a similar method was applied to acquire crack propagation in homogeneous models using the same geometry. The results of the application of a geostress ratio of 1:1.0, 1:1.5, and 1:1.9 are shown in Fig. 7 for the sake of comparison. The results indicate that for homogeneous models, crack initiation is monotonous, following conventional theory, i.e., the crack propagate steadily no obvious difference. This tendency implies that local resistance to crack propagation has significant difference if the rock media are heterogeneous. In addition, the branches on different sides of the wellbore would coalesce by breaking the elements along the wellbore circumference in the heterogeneous models, which is behavior that cannot be found in the homogeneous models.

Our numerical results show that material heterogeneity has great effect on crack initiation and coalescence near the wellbore when the geostress ratio is <1.7. If the applied geostress difference is high, the geostress difference has greater effect than material heterogeneity in governing the initiation and subsequent propagation of cracks. The geostress ratio of 1:1.7 seems to be the threshold below which material heterogeneity plays the dominant role in governing crack initiation.

Fig. 8 illustrates the tendency of the breakdown pressure with increasing geostress ratio. The breakdown pressure is a critical factor for characterizing hydrofracturing performance. In our simulation, the moment of specimen breakdown was defined as the occurrence of observable initial crack within a hydrofracturing specimen. The dichotomy method was adopted to determine the breakdown pressure. As aforementioned, the crack initiation and propagation was numerically treated as a quasi-static process, which allows us to increase water pressure step by step numerically until the specimen was broken down. The increment was 5 MPa for each pressure step. Once the initial crack first emerged with increasing pressure, we halved the step load and proceeded to check if the crack propagated. If not, we then increased water pressure to three fourths of its original value and applied to the elements to check whether the crack propagated. If yes, we decreased water pressure to one fourth of its original value to check if crack emerged. Repeating this dichotomy method we approached to the desired breakdown pressure that caused the initial failure of elements.

The calculation results indicate that the breakdown pressure decreases with increasing the maximum horizontal geostress, which coincides with the results of conventional theories and

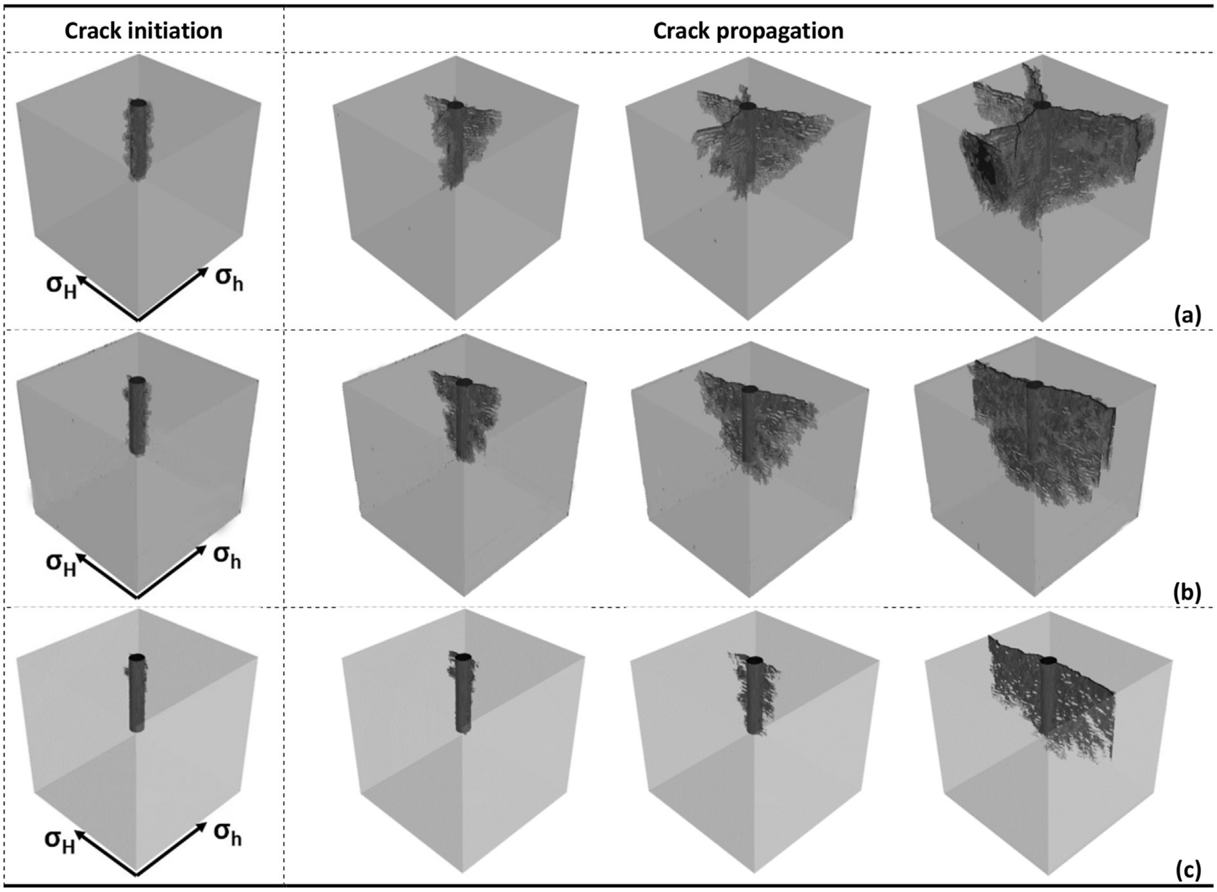


**Fig. 7.** 3D morphologies of hydrofracturing cracks in homogeneous models under different loading steps. Rows (***a***) to (***c***) show the results for geostress ratios of 1:1.0, 1:1.5, and 1:1.9, respectively.

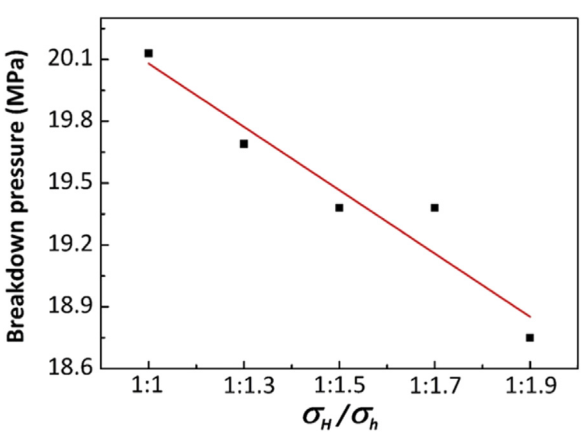


**Fig. 8.** Numerical results of breakdown pressure versus geostress difference.

suggested by most studies (e.g. Hubbert and Willis, 1957; Guo et al., 1993; Zhang et al., 2016, etc.). However, most previous studies focused on homogeneous samples rather than heterogeneous samples. The variation amplitude of the breakdown pressure of our simulation is not as big as that of conventional theories. This phenomenon may result from the coupled effects of material heterogeneity and horizontal geostress difference on the characterizations of breakdown pressure. In other words, for a heterogeneous sample, heterogeneous gravels significantly affect crack initiation and propagation, narrowing the gap in breakdown pressures. The material heterogeneity affects the variation of breakdown pressures more than the geostress difference for heterogeneous rocks. This has been verified by our previous experimental results (Liu et al., 2016; Ju et al., 2016).

## 4. Experimental verification

The experimental results in the previous studies were employed to verify the simulation results. The detailed discussion can refer to the reference (Liu et al., 2016). The samples in the experiments contained the same gravels distribution. The external conditions were also the same, including the vertical stress applied, horizontal geostress ratios, and stable injection rate. To investigate the fracture patterns, 3D morphologies of the cracks were reconstructed using the CT technique in combination with image processing methods. The reconstruction results are illustrated in Fig. 9. The experimental studies showed that the geostress ratio of 1:1.7 seems to be a threshold value for multiple fracture patterns to emerge, which confirms the numerical results of this study. However, there were some differences in the final crack morphologies between the experimental and numerical results. In the numerical simulation, once the geostress ratio was >1:1, a principal crack formed without many multiple branches, which contrasted with the multiple cracks observed in the experiments. In fact, crack propagation was affected by both the initial azimuth geostress conditions and the net pressure within the cracks. The reason for this difference could be that the water pressure within the fracture was applied uniformly onto the fracture surface in the numerical model, while the

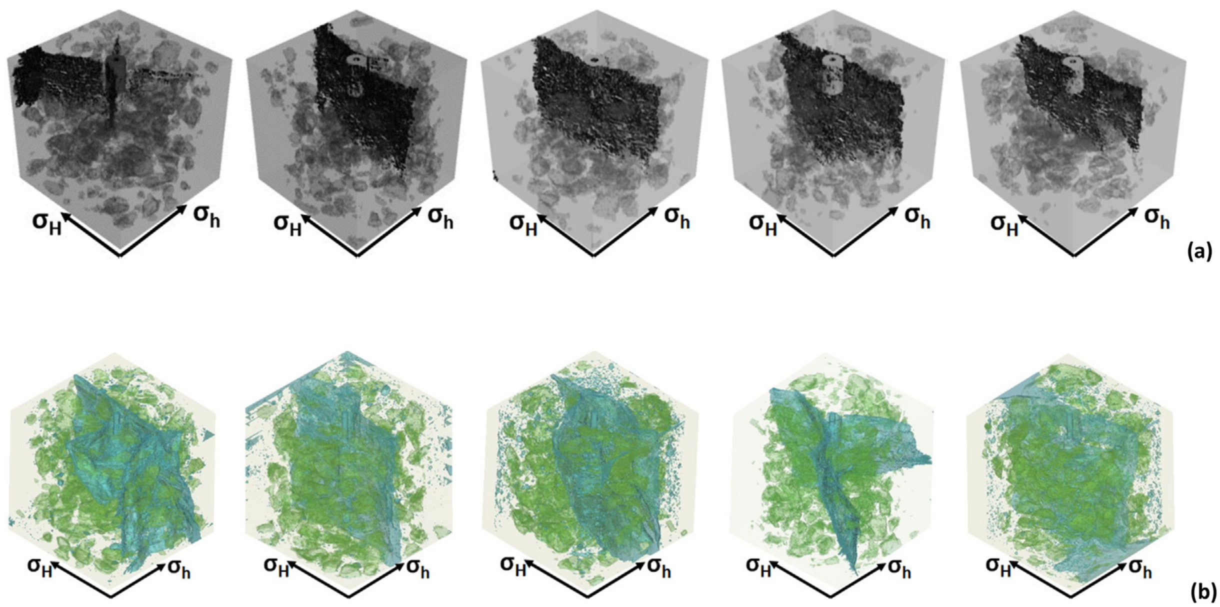


**Fig. 9.** Comparison of hydrofracturing crack morphologies between numerical and experimental results. Columns from left to right refer to geostress ratios ranging from 1:1.0 to 1:1.9. (***a***) Crack morphologies in the numerical results and (***b***) the experimental results at the final stage of the hydrofracturing process.

net pressure within the initial crack in the experimental models might be more complicated. However, for lack of an on-site CT scanning of hydrofracturing processes, the stepwise process of crack initiation and propagation inside the specimen cannot be experimentally captured in real time to date. Only the finishing fracture pattern can be imaged using the current CT technique. This causes difficulties to quantitatively compare the stepwise process of crack initiation and propagation between numerical results and experimental data. The on-site real time CT technology could be a promising option for overcoming this problem.

It is noteworthy that in both the numerical and the experimental results, crack braches combined with each other by breaking the solid near the side of the wellbore. Theoretically, cylindrical cracks initiate around casing surfaces owing to the difference in material properties between rock matrices and metals. As aforementioned above, a packer was placed on the top of the wellbore. In this case, it was found that the pressurized crack is not a pure mode-I opening crack and has apparent shear forces developed along the fracture front (Taleghani and Klimenko, 2015). It results from the coupled effect of shear forces and tensile forces. The non-planar cracks around the wellbore were observed in our previous CT tests. In addition, when the horizontal geostress ratio was sufficiently large (such as 1:1.9), the crack morphologies of the numerical simulation and the experimental works were similar, i.e., crack faces were smooth in the vertical plane.

## 5. Conclusions

This study conducted numerical simulations to investigate crack initiation and propagation processes in heterogeneous material. A CDEM algorithm was used to reveal the crack morphologies at different stages under the coupled effects of horizontal geostress differences and material heterogeneity. Numerical models that represented actual components distributions in the rock media were constructed and used in the simulations. A few homogeneous numerical models without embedded gravels were also considered for the purposes of comparison. To verify the validity of the simulation results, experimental results achieved in previous works were used for comparison with the final crack morphologies generated by the numerical simulations. The principal conclusions are as follows.

(1) Material heterogeneity had significant influence on crack initiation. Cracks emerged at various azimuths around the vertical wellbore, and microcracks coalesced to form main branches during the propagation process. Heterogeneous media provided different resistance in different crack propagation trajectories, which resulted in different crack volumes. Conversely, only a few initial tensile cracks developed in the homogeneous model and the branches on different sides of the wellbore propagated equally without obvious volume differences.

(2) The geostress ratio controlled crack propagation. A geostress ratio of 1:1.7 appeared to be the threshold below which material heterogeneity rather than geostress difference played the dominant role in governing crack initiation. However, cracks propagated in multiple directions under geostress ratio of 1:1. When the geostress was no longer equivalent, a double-wing crack formed and the breakdown pressure declined as the geostress ratio increased.

(3) The numerical simulations were verified by the experimental results. Although multiple crack patterns were not obtained in the numerical simulations under geostress ratios >1, the combined patterns of the branches were similar to the experimental results. When the geostress ratio was >1:1.7, a smooth planner crack was obtained in both the numerical and the experimental works.

**Acknowledgements**

The authors gratefully acknowledge the financial support of the National Natural Science Foundation of China [Grants 51374213 and 51674251], National Natural Science Fund for Distinguished Young Scholars of China [Grant 51125017], Science Fund for Creative Research Groups of the National Natural Science Foundation of China [Grant 51421003], Fund for Creative Research and Development Group Program of Jiangsu Province [Grant 2014-27], and the Priority Academic Program Development of Jiangsu Higher

Education Institutions (Grant PAPD2014). The authors would also like to express their gratitude to the editors and the anonymous reviewers for their valuable comments and suggestions, which have greatly improved this paper.

## References


Adriaensens, P., Storme, L., Carleer, R., Vanderzande, D., Gelan, J., Litvinov, V.M., Marissenf, R., 2000. Visualization of tensile stress induced material response at a crack tip in polymers under critical load by NMR imaging. Macromolecules 33 (13), 4836–4841.

Al-Busaidi, A., Hazzard, J., Young, R., 2005. Distinct element modeling of hydraulically fractured Lac du Bonnet granite. J. Geophys. Res. Solid Earth (1978–2012) 110 (110), 351–352.

Almi, S., Maso, G.D., Toader, R., 2014. Quasi-static crack growth in hydraulic fracture. Nonlinear Anal. 109, 301–318.

Bouchard, P.O., Bay, F., Chastel, Y., Tovena, I., 2000. Crack propagation modelling using an advanced remeshing technique. Comput. Method Appl. M 189 (3), 723–742.

Bunger, A.P., Kear, J., Dyskin, A.V., Pasternak, E., 2015. Sustained acoustic emissions following tensile crack propagation in a crystalline rock. Int. J. Fract. 193 (1), 87–98.

Chen, Y., Nagaya, Y., Ishida, T., 2015. Observations of fractures induced by hydraulic fracturing in anisotropic granite. Rock Mech. Rock Eng. 48 (4), 1455–1461.

Cipolla, C., Weng, X., Mack, M., Ganguly, U., Gu, H., Kresse, O., Cohen, C., 2012. Integrating microseismic mapping and complex fracture modeling to characterize fracture complexity. In: SPE Hydraulic Fracturing Technology Conference. Society of Petroleum Engineers. SPE140185.

Cundall, P.A., Strack, O.D.L., 1979. A discrete numerical mode for granular assemblies. Géotechnique 29 (1), 47–65.

Dong, C.Y., De Pater, C.J., 2001. Numerical implementation of displacement discontinuity method and its application in hydraulic fracturing. Comput. Method. Appl. M 191 (8–10), 745–760.

Fatahi, H., Hossain, M.M., Fallahzadeh, S.H., Mostofi, M., 2016. Numerical Simulation for the Determination of Hydraulic Fracture initiation and breakdown pressure using distinct element method. J. Nat. Gas. Sci. Eng. 1–14.

Fouche, O., Wright, H., Cleac'H, J.M.L., Pellenard, P., 2004. Fabric control on strain and rupture of heterogeneous shale samples by using a non-conventional mechanical test. Appl. Clay Sci. 26, 367–387.

Gomaa, A.M., Zhang, B., Chen, J., Qu, Q., Nelson, S., 2014. Using NMR technology to study the flow of fracture fluid inside shale formation. In: SPE International Symposium and Exhibition on Formation Damage Control. Society of Petroleum Engineers, pp. 667–680.

Guo, C., Xu, J., Wei, M., Jiang, R., 2015. Experimental study and numerical simulation of hydraulic fracturing tight sandstone reservoirs. Fuel 159, 334–344.

Guo, F., Morgenstern, N.R., Scott, J.D., 1993. Interpretation of hydraulic fracturing breakdown pressure. Int. J. Rock Mech. Min. Sci. Geomech. Abstr. 30 (6), 617–626.

Gutierrez, M.G., Sanchez, A.C., Rios, A., Arguello, L., 2010. Microseismic hydraulic fracture monitoring to determine the fracture geometry in Coyotes field, Chicontepec. In: SPE Latin American and Caribbean Petroleum Engineering Conference. Society of Petroleum Engineers. SPE 139155.

Hampton, J.C., Hu, D., Matzar, L., Gutierrez, M., 2014. Cumulative volumetric deformation of a hydraulic fracture using acoustic Emission and micro-CT imaging. In: 48th US Rock Mechanics/Geomechanics Symposium. American Rock Mechanics Association. ARMA 7041.

Hiyama, M., Shimizu, H., Ito, T., Tamagawa, T., Tezuka, K., 2013. Distinct element analysis for hydraulic fracturing in shale-Effect of brittleness on the fracture propagation. In: 47th U.S. Rock Mechanics/Geomechanics Symposium. American Rock Mechanics Association. ARMA 659.

He, S., Jiang, Y., Conrad, J.C., Qin, G., 2015. Molecular simulation of natural gas transport and storage in shale rocks with heterogeneous nano-pore structures. J. Petrol. Sci. Eng. 133, 401–409.

Hu, Y., Perdomo, M.E.G., Wu, K., Chen, Z., Zhang, K., Ji, D., Zhong, H., 2015. A novel model of brittleness index for shale gas reservoirs: confining pressure effect. In: SPE Asia Pacific Unconventional Resources Conference and Exhibition. Society of Petroleum Engineers, Brisbane, Australia.

Hubbert, M.K., Willis, D.G., 1957. Mechanics of hydraulic fracturing. Trans. AIME 210, 153–168.

Ju, Y., Zheng, J., Epstein, M., Sudak, L., Wang, J., Zhao, X., 2014. 3D numerical reconstruction of well-connected porous structure of rock using fractal algorithms. Comput. Method. Appl. M 279 (9), 212–226.

Ju, Y., Xing, M.X., Sun, H.F., 2013. Computer Program for Extracting and Analyzing Fractures in Rocks and Concretes. Software Copyright Registration #0530646. Beijing (in Chinese).

Ju, Y., Yang, Y.M., Chen, J.L., Liu, P., Dai, T., Guo, Y.C., Zheng, L.G., 2016. 3D reconstruction of low-permeability heterogeneous glutenites and numerical simulation of hydraulic fracturing behavior. Chin. Sci. Bull. 61, 82–93 (In Chinese).

Kaestner, A., Lehmann, E., Stampanoni, M., 2008. Imaging and image processing in porous media research. Adv. Water Resour. 31 (9), 1174–1187.

Li, L., Meng, Q., Wang, S., Li, G., Tang, C., 2013. A numerical investigation of the hydraulic fracturing behaviour of conglomerate in Glutenite formation. Acta Geotech. 8 (6), 597–618.

Li, Q., Xing, H., Liu, J., Liu, X., 2015. A review on hydraulic fracturing of unconventional reservoir. Petroleum 1 (1), 8–15.

Li, S.H., Zhao, M.H., Wang, Y.N., Rao, Y., 2004. A new numerical method for demblock and particle model. Int. J. Rock Mech. Min. Sci. 41 (3), 414–418.

Liu, H., Jiang, Z., Cao, Y., Wang, Y., 2010. Sedimentary characteristics and hydrocarbon accumulation of glutenite in the fourth member of Eogene Shahejie formation in Shengtuo area of Bohai Bay Basin, East China. Neurology 28 (28), 1039–1044.

Liu, H.Y., Roquete, M., Kou, S.Q., Lindqvist, P.A., 2004. Characterization of rock heterogeneity and numerical verification. Eng. Geol. 72 (1–2), 89–119.

Liu, P., Ju, Y., Ranjith, P.G., Zheng, Z.M., Chen, J.L., 2016. Experimental investigation of the effects of heterogeneity and geostress difference on the 3D growth and distribution of hydrofracturing cracks in unconventional reservoir rocks. J. Nat. Gas. Sci. Eng. (in press).

Moës, N., Dolbow, J., Belytschko, T., 1999. A finite element method for crack growth without remeshing. Int. J. Numer. Meth. Eng. 46 (1), 131–150.

Morita, N., Gray, K.E., Srouji, F.A.A., Jogi, P.N., 1992. Rock-property changes during reservoir compaction. SPE Form. Eval. 7, 197–205.

Nassir, M.J., Settari, A., Wan, R., 2010. Modeling shear dominated hydraulic fracturing as a coupled fluid-solid interaction. In: International Oil and Gas Conference and Exhibition. Society of Petroleum Engineers, pp. 8–10.

Potyondy, D.O., Cundall, P.A., 2004. A bonded-particle model for rock. Int. J. Rock Mech. Min. 41 (8), 1329–1364.

Rashid, M.M., 1998. The arbitrary local mesh replacement method: an alternative to remeshing for crack propagation analysis. Comput. Methods Appl. Mech. Eng. 154 (1), 133–150.

Renard, F., Bernard, D., Desrues, J., Ougier-Simonin, A., 2009. 3D imaging of fracture propagation using synchrotron X-ray microtomography. Earth Planet. Sci. Lett. 286 (s 1–2), 285–291.

Sarmadivaleh, M., Rasouli, V., 2015. Test design and sample preparation procedure for experimental investigation of hydraulic fracturing interaction modes. Rock Mech. Rock Eng. 48 (1), 93–105.

Shimizu, H., Hiyama, M., Ito, T., Tamagawa, T., Tezuka, K., 2014. Flow-coupled DEM simulation for hydraulic fracturing in pre-fractured rock. In: 48th US Rock Mechanics/Geomechanics Symposium. American Rock Mechanics Association. ARMA 7365.

Shimizu, H., Murata, S., Ishida, T., 2011. The distinct element analysis for hydraulic fracturing in hard rock considering fluid viscosity and particle size distribution. Int. J. Rock Mech. Min. 48 (5), 712–727.

Taleghani, A.D., Klimenko, D., 2015. An analytical solution for micro-annulus cracks developed around a wellbore. J. Energ. Resour. ASME 137, 63–65.

Tang, C., Tham, L., Lee, P., Yang, T., Li, L., 2002. Coupled analysis of flow, stress and damage (FSD) in rock failure. Int. J. Rock Mech. Min. 39 (4), 477–489.

Wang, L., Li, S., Zhang, G., Ma, Z., Zhang, L., 2013. A GPU-based parallel procedure for nonlinear analysis of complex structures using a coupled FEM/DEM approach. Math. Probl. Eng. 2013 (9), 841–860.

Wang, Y., 2013. Numerical modelling of heterogeneous rock breakage behaviour based on texture images. Min. Eng. 74, 130–141.

Wang, Y., Zhao, M., Li, S., Wang, J.G., 2005. Stochastic structural model of rock and soil aggregates by continuum-based discrete element method. Sci. China 48 (S1), 95–106 (In Chinese).

Wong, T.F., Wong, R.H.C., Chau, K.T., Tang, C.A., 2006. Microcrack statistics, Weibull distribution and micromechanical modeling of compressive failure in rock. Mech. Mater. 38 (7), 664–681.

Yang, T.H., Tham, L.G., Tang, C.A., Liang, Z.Z., Tsui, Y., 2004. Influence of heterogeneity of mechanical properties on hydraulic fracturing in permeable rocks. Rock Mech. Rock Eng. 37 (4), 251–275.

Yin, T.B., Shu, R.H., Li, X.H., Wang, P., Liu, X. l, 2016. Comparison of mechanical properties in high temperature and thermal treatment granite. Trans. Nonferr. Metal Soc. 26 (7), 1926–1937.

Yue, Z.Q., Chen, S., Tham, L.G., 2003. Finite element modeling of geomaterials using digital image processing. Comput. Geotech. 30 (5), 375–397.

Zhang, B., Li, X., Zhang, Z., Wu, Y., Wu, Y., Wang, Y., 2016. Numerical investigation of influence of in-situ stress ratio, injection rate and fluid viscosity on hydraulic fracture propagation using a distinct element approach. Energies 9, 140.

Zhang, P., Zhang, J., Xie, J., Lee, Y.I., Zhang, M., Ding, F., Yuan, Y., Li, J., Zhang, X., 2014. Deposition and diagenesis of steep-slope glutenite reservoirs: Shengtuo field, eastern China. Energ. Explor. Exploit. 32 (3), 483–502.

Zhang, X., Jeffrey, R.G., Thiercelin, M., 2007. Deflection and propagation of fluid-driven fractures at frictional bedding interfaces: a numerical investigation. J. Struct. Geol. 29 (3), 396–410.

Zhou, D.S., Zheng, P., He, P., Peng, J., 2016. Hydraulic fracture propagation direction during volume fracturing in unconventional reservoirs. J. Petrol. Sci. Eng. 141, 82–89.

Zou, Y.S., Zhang, S.C., Zhou, T., Zhou, X., Guo, T.K., 2016. Experimental investigation into hydraulic fracture network propagation in gas shales using CT scanning technology. Rock Mech. Rock Eng. 49 (1), 33–45.